THE JOURNAL OF PHYSICAL CHEMISTRY B

Article

pubs.acs.org/JPCB

Quantum Process Tomography Quantifies Coherence Transfer Dynamics in Vibrational Exciton

Lev Chuntonov*,‡ and Jianqiang Ma‡

Ultrafast Optical Processes Laboratory, Department of Chemistry, University of Pennsylvania, Philadelphia, PA 19104, United States

Supporting Information

ABSTRACT: Quantum coherence has been a subject of great interest in many scientific disciplines. However, detailed characterization of the quantum coherence in molecular systems, especially its transfer and relaxation mechanisms, still remains a major challenge. The difficulties arise in part because the spectroscopic signatures of the coherence transfer are typically overwhelmed by other excitation-relaxation processes. We use quantum process tomography (QPT) via two-dimensional infrared spectroscopy to quantify the rate of the elusive coherence transfer between two vibrational exciton states. QPT retrieves the dynamics of the dissipative quantum system directly from the experimental observables. It thus serves as an experimental alternative to theoretical models of the system−bath interaction and can be used to validate these theories. Our results for coupled carbonyl groups of a diketone molecule in chloroform, used as a benchmark system, reveal the nonsecular nature of the interaction between the exciton and the Markovian bath and open the door for the systematic studies of the dissipative quantum systems dynamics in detail.

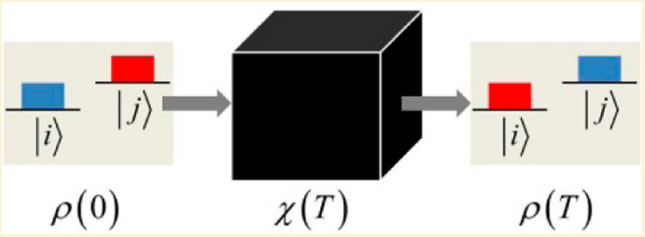

INTRODUCTION

Quantum coherence was found to play an important role in natural and artificial molecular systems.[1−6] Manipulation and control of the coherence is of high interest in many different fields of science.[7] Ultrafast two-dimensional infrared vibrational spectroscopy (2D-IR) explores coherent excitations of molecular quantum states and tracks their time-dependent relaxation.[8−14] It has been proved a powerful tool to study molecular structure and dynamics in a broad range of problems.[15−25] Strong coupling between the nearly degenerate local states of the molecule leads to new delocalized quantum states known as molecular excitons.[26,27] Coherent dynamics and relaxation of excitons is highly sensitive to the way the interaction with the environment perturbs the system.[1−3,5,11,16,28−30] For the case of molecules in solution, such perturbations are caused by the fluctuating bath of solvent molecules.[31]

As opposed to the well-known relaxation processes such as vibrational lifetime, rotational diffusion, and pure dephasing,[29,32−35] the mechanisms of the relaxation by the excitation transfer has not been fully explored.[28,31−34] When the quantum states of the vibrational exciton are represented in the Liouville space by elements of the reduced density matrix ρ_{ij}, where indices i and j are the vibrational one-exciton transitions, the corresponding relaxation channels are the transfer between the populations and coherences of $\hat{\rho}$. The transfer between the different populations and between the coherences may occur for the coupled vibrational modes at room temperature if the thermal fluctuations of the bath provide the energy required for the transfer.[32,33,36−41]

Detailed characterization of all relaxation pathways is highly important for the better understanding of the dissipative quantum system dynamics in the condensed phase and further exploring (and even control) it with novel spectroscopic methods. The transfer of the population and coherence within the one-exciton vibrational manifold cannot be readily characterized by the standard methods of multidimensional spectroscopy, especially when the transfer states are nearly degenerated.[32,33,40−43] The transfer between the populations $|i\rangle\langle i|$ and $|j\rangle\langle j|$ is manifested in the monotonous growth of the cross-peaks' amplitude with respect to the amplitude of the diagonal peaks observed in the waiting time series of 2D-IR spectra.[23,37−39,44,45] In the case of nearly degenerate vibrational modes, the population transfer can be challenging to characterize because the cross-peaks cannot be easily separated.[40,41] The characterization of the transfer between the coherences $|i\rangle\langle j|$ and $|j\rangle\langle i|$ is even more challenging because such a transfer neither generates new peaks in the 2D spectrum nor beats at new frequencies during the waiting time.[32,33]

In the multidimensional spectroscopy, interpretation of the experimental results strongly relies on the models used to describe the molecular system and its interaction with the bath. Such description can be either phenomenological or based on stochastic models, molecular dynamics simulations, or quantum-mechanical methods.[8,46−48] Among different approaches, response functions method derived with the time-dependent perturbation theory is the most intuitive one and it

Received: July 29, 2013
Revised: September 25, 2013

   dx.doi.org/10.1021/jp4075493 | J. Phys. Chem. B XXXX, XXX, XXX−XXX

is widely used to understand experimental 2D-IR spectra.[8] However, strict derivation of the response functions does not involve excitation transfer effects, including the transfer of the vibrational coherence. An alternative to modeling a system−bath interaction observed through the excited states relaxation in a nonlinear spectroscopic experiment is the approach of quantum process tomography (QPT)[49−51] adapted from the field of quantum information by Aspuru-Guzik and co-workers.[52−54] QPT has the unique ability of giving a model-free characterization of the evolution of the dissipative quantum system, and it can be used to validate proposed theoretical models and phenomenological constants.

In the present study, we applied QPT via 2D-IR spectroscopy to quantify excitation transfer dynamics in the vibrational exciton in 1,3-cyclohexanedione (CHD) molecule solvated in chloroform. Here, in addition to the transfer of the vibrational population, QPT allowed us to reveal dynamics of the coherence transfer, which is masked by the contributions from the photoinduced pathways that do not involve transfer. Note, however, that present QPT implementation is partial because the processes of transfer between the vibrational population and coherence and vice versa cannot be observed as the corresponding ensemble-averaged signal vanishes, as discussed below.[49,50] We found that in the regime of fast transfer and slow dephasing rates, which are dictated by the dynamics of the solvation shell, the system evolution fully agrees with the solution of the equation of motion for the exciton coupled to the Markovian bath. The corresponding equation of motion includes both secular and nonsecular terms describing the transfer of the vibrational population and coherence respectively.[29] We anticipate that these findings are of high importance in the general context of multidimentional spectroscopy, which is frequently used to study systems where the transfer phenomena play significant roles.

As opposed to electronic excitons,[1−3,55] where the QPT by 2D spectroscopy was originally proposed,[49,50] vibrational excitons typically show lifetime and orientational relaxation on the time scale of the excitation transfer, and their reliable characterization in such situations provides an additional experimental challenge.[43] Here we used full spectroscopic characterization of the CHD in chloroform to extract the molecular dynamics constants essential for QPT. The effectiveness of our implementation of the QPT protocol is confirmed by test reconstructions of the dynamics from numerically simulated series of 2D-IR spectra.

EXPERIMENTAL METHODS

The 2D-IR experiment was carried with four linearly polarized ca. 75 fs mid-IR pulses in the BOXCARS geometry. Polarization was rotated by true zero-order waveplates. High-extinction wire-grid polarizers (Specac Ltd., extinction ratio ca. 1:700) were placed right before the focusing lens to avoid depolarization upon reflections. An additional polarizer on the signal beam was placed immediately after the sample cell. The heterodyne pulse preceding the excitation pulses by 1 ps was overlapped with the signal dispersed onto the liquid nitrogen-cooled array detector coupled to the spectrograph.

A solution of ca. 0.1 M of 1,3-cyclohexanedione (97%, Aldridch) in chloroform was placed between CaF_2 windows with 25 μm spacer. In all experiments, the optical density of the sample was kept below 0.2.

Quantification of the excitation transfer dynamics of the vibrational exciton demonstrated in the present work requires characterization of its vibrational lifetime and orientational relaxation. This information is consistently obtained by the established procedures from the waiting-time series of the 2D-IR spectra. Vibrational lifetime is obtained from the relaxation of the polarization-isotropic signals corresponding to the amplitudes of the diagonal peaks, and the orientational relaxation from their polarization anisotropy. The corresponding experimental data and its analysis are shown in the Supporting Information. The resulting values of the vibrational lifetime T_1 = 3 ps and orientational relaxation time τ_D = 30 ps were used in the QPT analysis.

QPT by 2D-IR Spectroscopy. In a 2D-IR experiment, the initial state of the system, $\rho_{ij}(0)$, is prepared by the interaction with first two femtosecond pulses delayed by the time interval τ. The system evolves while it interacts with the solvent bath during the waiting time interval T into a final state $\rho_{ij}(T)$, which is probed by the second pair of pulses separated by time interval t. Note that in addition to the excited state populations $|i\rangle\langle i|$ and coherences $|i\rangle\langle j|$, the ground state population $|0\rangle\langle 0|$ is also prepared by the first two pulses. However, $|0\rangle\langle 0|$ is not involved in the population transfer because of the high energy separation between the quantum states of the molecule $|0\rangle$ and $|i\rangle$, $|j\rangle$.

The goal of the QPT discussed in the present work is to characterize the dynamics of one-exciton quantum states of CHD, which evolve during the waiting time T of the experiment by means of the process matrix $\hat{\chi}(T)$

$$\rho_{ij}(T) = \sum_{kl} \chi_{ij,kl}(T)\rho_{kl}(0) \tag{1}$$

The process matrix is, therefore, a linear transformation known to fully describe the system evolution independent of its initial state. Here we reconstruct the process matrix by analysis of the spectroscopic observables measured by polarization-selective 2D-IR spectroscopy.[56]

The heterodyned photon echo signal measured in the 2D-IR experiment is generated by the third-order nonlinear polarization of the sample $P^{(3)}_{\mathrm{ABCD}}$, which is the expectation value of the transition dipole moment operator $\hat{\mu}(t')$ given by $P(t') = \langle\hat{\mu}(t')\hat{\rho}(t')\rangle$. The signal field is emitted in the direction satisfying the phase-matching conditions $\mathbf{k}_S = -\mathbf{k}_1 + \mathbf{k}_2 + \mathbf{k}_3$, where the subscripts enumerate the wave vectors of the femtosecond pulses. In the 2D spectroscopy, the corresponding signal is referred to as rephrasing.[9,10] Assuming that the pulses are infinitely short and linearly polarized along the directions A, B, C, and D in the lab frame, the photon echo signal is given by

$$S^{\mathrm{ABCD}}(\omega_\tau, T, \omega_t) \propto -i\int_0^\infty e^{-i\omega_\tau\tau}\mathrm{d}\tau\int_0^\infty e^{i\omega_t t}\mathrm{d}t P^{(3)}_{\mathrm{ABCD}}(\tau, T, t) \tag{2}$$

Depending on exciton's transition frequencies, 2D-IR spectrum $S^{\mathrm{ABCD}}(\omega_\tau,T,\omega_t)$ exhibits diagonal peaks corresponding to the case where the same exciton state is pumped and probed and cross-peaks where one of the exciton states is pumped and a different (coupled) state is probed.

A time-dependent third-order perturbation theory description of the system includes density matrix evolution during the time intervals τ and t, reflected in the lineshapes of the 2D spectral peaks.[8−10] Unlike in the perturbative approach, within the QPT formalism, only the system dynamics during the waiting time is of interest such that the spectral lineshapes are of less importance and $\rho(T)$ is given by eq 1.[49,50] When only the peak amplitudes are considered, the spectrum is given by

dx.doi.org/10.1021/jp4075493 | J. Phys. Chem. B XXXX, XXX, XXX−XXX

$$S^{\mathrm{ABCD}}(\omega_\tau, T, \omega_t) = \sum_{ij} S_{ij}^{\mathrm{ABCD}}(T) \tag{3}$$

where $S_{ij}^{\mathrm{ABCD}}(T) = S^{\mathrm{ABCD}}(\omega_i,T,\omega_j)$, and ω_i is the resonance frequency of the one-exciton mode i. In the following, we assume that there is no significant spectral diffusion in the system, such that the lineshapes do not change during the waiting time. We also assume that the combination mode of the exciton does not interfere with one-exciton transitions.

Adapting the protocol of refs 49 and 50 to 2D-IR spectroscopy, the amplitudes $S_{ij}(T)$ are expressed in terms of the elements of the process matrix as

$$\begin{aligned} S_{ii}^{\mathrm{ABCD}}(T) = {} & 2\mu_i^4\langle i_\mathrm{A} i_\mathrm{B} i_\mathrm{C} i_\mathrm{D}\rangle\chi_{ii,ii}(T)\mathrm{e}^{-T/T_1^{(i)}} \\ & + \mu_i^4\langle j_\mathrm{A} j_\mathrm{B} i_\mathrm{C} i_\mathrm{D}\rangle\chi_{jj,ii}(T)\mathrm{e}^{-T/T_1^{(i)}} \\ & + \mu_i^2\mu_j^2\langle i_\mathrm{A} j_\mathrm{B} j_\mathrm{C} i_\mathrm{D}\rangle\chi_{ij,ji}(T)\mathrm{e}^{-T/2T_1^{(i)}-T/2T_1^{(j)}} \end{aligned} \tag{4}$$

$$\begin{aligned} S_{ij}^{\mathrm{ABCD}}(T) = {} & \mu_i^2\mu_j^2\langle i_\mathrm{A} i_\mathrm{B} j_\mathrm{C} j_\mathrm{D}\rangle\chi_{ii,ii}(T)\mathrm{e}^{-T/T_1^{(i)}} \\ & + \mu_i^2\mu_j^2\langle i_\mathrm{A} i_\mathrm{B} j_\mathrm{C} j_\mathrm{D}\rangle\chi_{jj,ii}(T)(\mathrm{e}^{-T/2T_1^{(i)}} + e^{-T/2T_1^{(j)}}) \\ & + \mu_i^2\mu_j^2\langle i_\mathrm{A} j_\mathrm{B} i_\mathrm{C} j_\mathrm{D}\rangle\chi_{ij,ij}(T)\mathrm{e}^{-T/2T_1^{(i)}-T/2T_1^{(j)}} \end{aligned} \tag{5}$$

where $T_1^{(i)}$is the vibrational lifetime of the state i with the transition dipole moment μ_i, and $\langle i_\mathrm{A} j_\mathrm{B} k_\mathrm{C} l_\mathrm{D}\rangle$are the orientational factors[57] corresponding to the Liouville pathway $ijkl$. In the derivation, we assumed the detailed balance of elements of $\chi(T)$ and stationarity of the ground state population $|0\rangle\langle 0|$ prepared by the first two pulses: $\chi_{00,00}(T) = \chi_{ii,ii}(T) + \chi_{jj,ii}(T) = 1$.[49,50] Note that only the one-exciton manifold is included in the discussion and that the coupling between the populations and coherences of $\hat{\rho}$ is neglected as it is not observed in the isotropic-averaged signal (i.e., ensemble-averaged factors $\langle i_\mathrm{A} i_\mathrm{B} i_\mathrm{C} j_\mathrm{D}\rangle = \langle i_\mathrm{A'} i_\mathrm{B'} j_\mathrm{C'} i_\mathrm{D'}\rangle = \langle i_\mathrm{A''} j_\mathrm{B''} i_\mathrm{C''} i_\mathrm{D''}\rangle = \langle j_\mathrm{A'''} i_\mathrm{B'''} i_\mathrm{C'''} i_\mathrm{D'''}\rangle$=0 for the polarization conditions considered in this work).[49,57] QPT is performed by solving a linear system of eqs 4−5 for waiting time series of 2D-IR spectra carried out under different polarization conditions A, B, C, and D. At least two polarization conditions from the set ⟨XXXX⟩ = ⟨YYXX⟩ + ⟨XYYX⟩ + ⟨YXYX⟩ are required for the system 4−5 to be determined.[57]

RESULTS AND DISCUSSION

Vibrational Exciton in CHD. Carbonyl groups in 1,3-cyclohexanedione molecule constitute a homodimer, which forms a vibrational exciton. The corresponding quantum states are manifested by two resonance peaks at ω_i = 1710 cm^{-1} (mode i) and ω_j =1734 cm^{-1} (mode j) as shown in the linear absorption spectrum in Figure 1a. The ratio of the associated transition dipole moments is found from the peak area to be μ_i^2/μ_j^2 = 3. This ratio corresponds to the relative magnitudes of the diagonal peaks, which appear at ($\omega_\tau = \omega_t = \omega_i$) and ($\omega_\tau = \omega_t = \omega_j$) in the 2D-IR spectrum of $S_{ii}^{\mathrm{YYXX}}(0)/S_{jj}^{\mathrm{YYXX}}(0) \propto \mu_i^4/\mu_j^4$ = 9 as seen in Figures 1b,c, where the absorptive and photon-echo 2D-IR spectra are shown for polarization conditions ⟨YYXX⟩. We choose to show here the spectrum corresponding to this particular polarization because it better illustrates the cross-peaks, which appear at ($\omega_\tau = \omega_i$, $\omega_t = \omega_j$) and ($\omega_\tau = \omega_j$, $\omega_t = \omega_i$).[57] The absorptive spectrum for polarization conditions of ⟨XXXX⟩ is also shown in Figure S1 of the Supporting Information. Positive peaks in the 2D-IR absorptive spectrum correspond to the one-exciton transitions, whereas negative peaks involve excited state absorption to either the second excited state or the combination state. In addition, in the photon-echo (rephasing) spectrum, each positive peak is accompanied by the negative dispersive contribution.[10] In the present work, only the positive peaks are considered. Because the anharmonicity of the exciton modes in CHD of Δ = 15 cm^{-1} is sufficiently large as compared to the linewidth (less than 10 cm^{-1}), the overlap between the negative and positive signal components does not affect the peak value of the positive peak significantly. In Figure S1 of the Supporting Information, we show a fit of the projection of 2D-IR spectrum on the ω_t axis to two Gaussian lineshapes with positive and negative amplitudes. The peak value of the positive Gaussian component differs by only ca. 2% from the corresponding value of the projection spectrum.

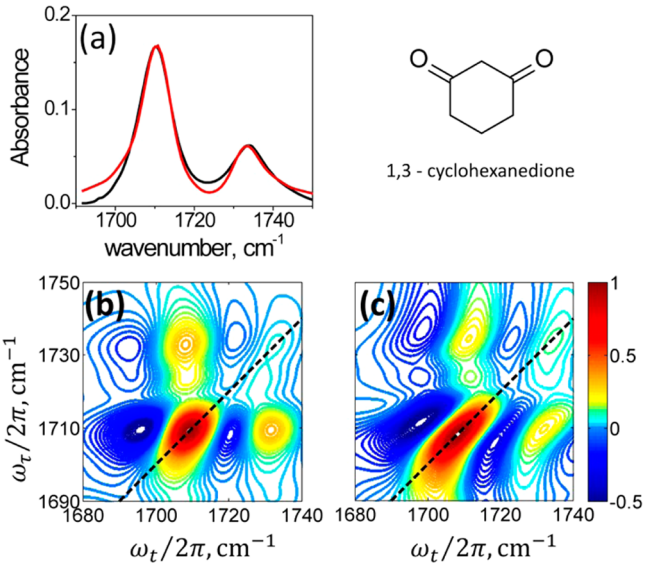

Figure 1. IR spectroscopy of CHD in chloroform. (a) Linear absorption spectrum: black line, experimental spectrum; red line, fit to the motional-narrowed lineshape with the vibrational lifetime and orientational relaxation contributions accounted for as determined by independent measurements. See text for the details. (b) Real part of the 2D-IR absorptive spectrum at T = 0 fs for ⟨YYXX⟩ polarization conditions. Positive contours indicate one-exciton manifold transitions. Dashed line is the diagonal line. (c) Real part of the 2D-IR photon-echo (rephasing) spectrum $S^{\mathrm{YYXX}}(\omega_\tau,T,\omega_t)$ at T = 0 fs.

For the case of the homodimer assumed here, the local modes of the carbonyl vibrations have similar energies and magnitudes of their transition dipole moments; the exciton mixing angle is $\pi/4$, such that the corresponding transition dipole moments are orthogonal. Orthogonality is confirmed by the amplitude ratio between the cross-peaks and diagonal peaks in the 2D-IR spectrum measured at T = 0, which is free from the waiting time dynamics.[14,58] In particular, for the spectrum in Figure 1c $S_{ii}^{\mathrm{YYXX}}(0)/S_{ij}^{\mathrm{YYXX}}(0) = 6\,\mu_i^2/\mu_j^2(P_2 + 5)$, where $P_2 = 1/2(3\cos^2\theta - 1)$ and θ is the angle between the transition dipole moments. The experimental value is $S_{ii}^{\mathrm{YYXX}}(0)/S_{ij}^{\mathrm{YYXX}}(0) \approx 4$ corresponding to $\theta = \pi/2$, which confirms the excitonic nature of the system.

QPT of Vibrational Exciton Dynamics: Experiment. The system of linear eqs 4−5, which relates the unknown elements of the process matrix $\chi_{ij,kl}(T)$ to the peak amplitudes $S_{ij}^{\mathrm{ABCD}}(T)$, was constructed for the waiting-time series of photon-echo spectra measured from T = 0 to T = 3.5 ps with 100 fs steps. For each value of T, a matrix equation $\underline{S}(T)$ =

dx.doi.org/10.1021/jp4075493 | J. Phys. Chem. B XXXX, XXX, XXX−XXX

$\underline{\boldsymbol{A}}(T)\underline{\chi}(T)$ was solved numerically using a procedure based on Gaussian elimination. Here, $\underline{S}(T)$ is a column vector of peak amplitudes $S_{ij}^{ABCD}(T)$, $\underline{\boldsymbol{A}}(T)$ is a coefficient matrix including transition dipole moments, orientational factors, rotational diffusion, and vibrational lifetime as defined by eqs 4−5, and $\underline{\chi}(T)$ is a column vector of the process matrix elements $\chi_{ij,kl}(T)$. The values of $S_{ij}^{ABCD}(T)$ were calculated numerically by averaging over the 1 cm^{-1} region around the resonance frequencies $\{\omega_\tau, \omega_t\} = \{\omega_i, \omega_j\}$in the 2D-IR spectra. The waiting time dependence of these signals for polarization conditions ⟨XXXX⟩ and ⟨YYXX⟩ are shown in Figure 2, and

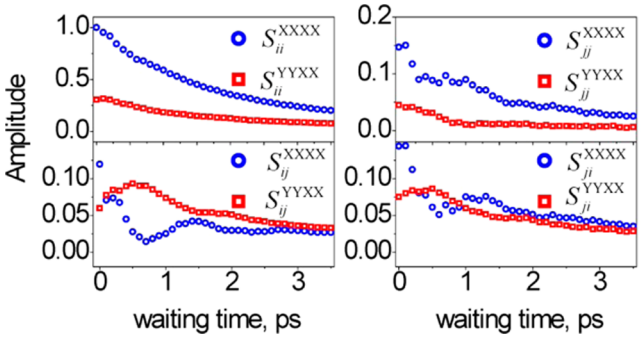

Figure 2. Real peak amplitudes $S_{ij}^{ABCD}(T)$ extracted from the waiting time series of the 2D-IR spectra of CHD in chloroform. The amplitudes are normalized to the value of $S_{ii}^{XXXX}(0)$.

the waiting time dependence of the elements of coefficient matrix $\underline{\boldsymbol{A}}(T)$ follows, for example, from ref 57 with the corresponding constants that we determined experimentally (see Experimental Methods section and Supporting Information). Here, we focus on the real part of $\chi_{ij,kl}(T)$ because it carries sufficient information to characterize the exciton dynamics in the present case. Extension of the QPT procedure to include also imaginary parts of $\chi_{ij,kl}(T)$ can readily be done, where necessary, as for example in electronic 2D spectroscopy.[55] Note that in the QPT analysis errors in the experimental signal, for example due to the fluctuation in the laser power, do not propagate to the subsequent time data points because the linear system of eqs 4−5 is constructed for each waiting time independently.

The waiting time dependence of the process matrix elements $\chi_{ij,kl}(T)$ reconstructed from the experimental data is shown in Figure 3. Because the vibrational lifetime and the orientational relaxation of the molecule are removed from the waiting time dependence of $\chi_{ij,kl}(T)$ (see eqs 4−5), the exciton dynamics represented by the process matrix is entirely due to the transfer processes and dephasing. The transfer of the population is manifested in the exponential decay of $\chi_{ii,ii}(T)$ and $\chi_{jj,jj}(T)$ and the exponential rise of the $\chi_{jj,ii}(T)$ and $\chi_{ii,jj}(T)$ elements, as seen in Figure 3a,b. On the other hand, the elements $\chi_{ij,ij}(T)$ and $\chi_{ji,ji}(T)$ describing the coherences oscillate with period of approximately 1.5 ps, which nearly matches the frequency difference between the exciton modes $\omega_{ij} = \omega_i - \omega_j = 24$ cm^{-1}, as seen from the absorptive spectrum in Figure 1. The oscillations decay exponentially with characteristic time of 1.0 ± 0.1 ps. In addition, the QPT reveals nonzero values of the coherence transfer matrix elements $\chi_{ji,ij}(T)$ and $\chi_{ij,ji}(T)$ as seen in Figure 3e,f, which also show damped oscillations (decay constant is 1.0 ± 0.1 ps) out-of-phase with respect to $\chi_{ij,ij}(T)$ and $\chi_{ji,ji}(T)$. Below, we interpret these observations on the basis of the kinetic model derived from the Liouville−von Neumann equation of motion for excitons coupled to a Markovian bath.

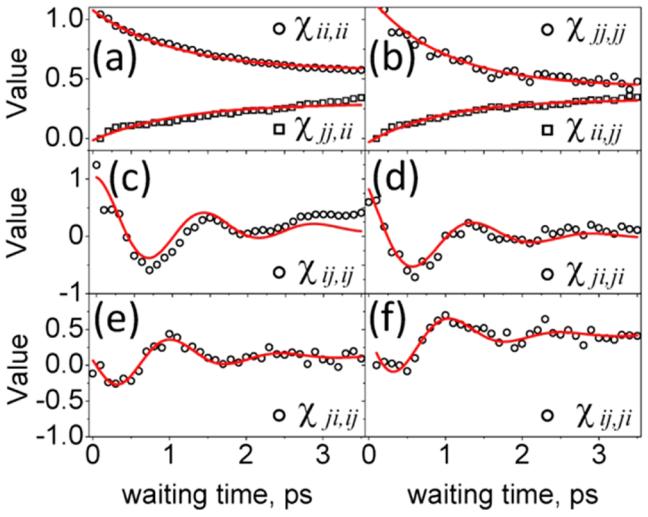

Figure 3. QPT of CHD: Experiment. Open dots are reconstructed elements of the process matrix $\chi_{ij,kl}(T)$. Red lines show fits of the results to the kinetic model on the basis of the Redfield's theory. See text for details.

Equations of Motion for Reduced Density Matrix. The waiting time dependent evolution of the reduced density matrix elements $\rho_{ij}(T)$ coupled to the Markovian solvent bath is described within the Liouville−von Neumann equation of motion

$$\dot{\rho}_{ij}(T) = -i\omega_{ij}\rho_{ij}(T) - \sum_{kl} R_{ij,kl}\rho_{kl}(T) \tag{6}$$

where $R_{ij,kl}$ are the elements of the Redfield's relaxation matrix.[29,31] Here, we assume that the population and coherence parts of the eq 6 are decoupled and can be treated separately.[37,40,41] Because we are particularly interested in the kinetics of the transfer processes and for simplicity, we do not account for the vibrational lifetime relaxation and rotational diffusion contributions. We also express the relaxation matrix elements with rate coefficients $k_{et} = 1/h^2\int_{-\infty}^{\infty}\langle V_{ji}(t)V_{ij}(0)\rangle e^{i\omega_{ij}t}dt$, where the brackets represent the trace over the bath degrees of freedom and $V_{ij}(t)$ is the matrix element of the system−bath interaction between the states $|i\rangle$ and $|j\rangle$.[29,31] A detailed balance requires that the population transfer rates $k_{ii,jj}$ and $k_{jj,ii}$ are related through the Arrhenius factor $k_{ii,jj} = Ak_{jj,ii} = Ak_{et}$, where $A = e^{h\omega_{ij}/k_BT} \approx 0.9$ for CHD at room temperature, and the coherence transfer rate constants are equal to $k_{ij,ji} = k_{ji,ij} = (1+A)k_{et}/2$.[29] The master equation for the population and coherence parts of $\rho(T)$ is given now by

dx.doi.org/10.1021/jp4075493 | J. Phys. Chem. B XXXX, XXX, XXX−XXX

$$\frac{\mathrm{d}}{\mathrm{d}T}\begin{pmatrix}\rho_{ii}\\ \rho_{jj}\\ \rho_{ij}\\ \rho_{ji}\end{pmatrix}=\begin{pmatrix}-k_{ii,jj} & k_{jj,ii} & 0 & 0\\ k_{ii,jj} & -k_{jj,ii} & 0 & 0\\ 0 & 0 & -k_{ij,ji}-\gamma-i\omega_{ij} & k_{ij,ji}\\ 0 & 0 & k_{ij,ji} & -k_{ij,ji}-\gamma+i\omega_{ij}\end{pmatrix}\begin{pmatrix}\rho_{ii}\\ \rho_{jj}\\ \rho_{ij}\\ \rho_{ji}\end{pmatrix} \tag{7}$$

where γ is the coherence dephasing rate. The solutions of eq 7 are

$$\rho_{ii}(T)=\frac{1}{k_{ii,jj}+k_{jj,ii}}[k_{jj,ii}+(k_{ii,jj}\,\rho_{ii}(0)-k_{jj,ii}\,\rho_{jj}(0))\mathrm{e}^{-(k_{ii,jj}+k_{jj,ii})T}] \tag{8}$$

and

$$\rho_{ij}(T)=\mathrm{e}^{-(k_{ij,ji}+\gamma)T}\left[\rho_{ij}(0)\left(\cos(\Omega T)-\frac{i\omega_{ij}}{\Omega}\sin(\Omega T)\right)+\rho_{ji}(0)\frac{k_{ij,ji}}{\Omega}\sin(\Omega T)\right] \tag{9}$$

where $\Omega=(\omega_{ij}^2-k_{ij,ji}^2)^{1/2}$. The expressions for ρ_{jj} and ρ_{ji} are obtained by interchanging the indices i and j.

The diagonal elements of the density matrix $\rho_{ii}(T)$ corresponding to the populations rise and decay exponentially depending on the initial conditions at the rate of $k_{ii,jj}+k_{jj,ii}$; at sufficiently large waiting time, $\rho_{ii}(T)$ reaches its equilibrium value. The off-diagonal elements $\rho_{ij}(T)$ corresponding to coherences have oscillatory terms, which are exponentially damped by dephasing and coherence transfer. In cases where the transfer rate constant $k_{ij,ji}$ is larger than ω_{ij}, the argument of the harmonic functions in eq 9 is purely imaginary, such that the solutions become combinations of hyperbolic functions. In the limiting case of degenerate vibrational modes (i.e., $\omega_{ij}=0$ and $k_{ii,jj}+k_{jj,ii}=2k_{et}$), the evolution of coherences follows exponential dynamics[40,41]

$$\rho_{ij}(T)=\frac{1}{2}\mathrm{e}^{-\gamma T}[\rho_{ij}(0)(1+\mathrm{e}^{-2k_{et}T})+\rho_{ji}(0)(1-\mathrm{e}^{-2k_{et}T})] \tag{10}$$

Rate Constants of Excitation Transfer Relaxation. Fits of the experimental results for $\chi_{ij,kl}(T)$ to the functions in eqs 8−9 are shown as red lines in Figure 3. The decay and buildup rates of the process matrix elements $\chi_{ii,ii}(T)$, $\chi_{jj,ii}(T)$,$\chi_{jj,jj}(T)$, and $\chi_{ii,jj}(T)$ corresponding to the top-left block of the relaxation matrix in eq 7 were globally fit to the functional form in eq 8, as seen in Figures 3a,b. The population transfer rate of $k_{ii,jj}=0.5\pm0.05$ ps^{-1} was found from the fit.

Fitting the time dependence of the coherence terms $\chi_{ij,ij}(T)$ and $\chi_{ji,ji}(T)$ in Figures 3c,d to the function in eq 9 results in the oscillation frequency of $\Omega=20\pm1$ cm^{-1}, which is smaller by 4 cm^{-1} than $\omega_{ij}=24$ cm^{-1} that was observed in the absorption spectrum in Figure 1. This difference between the values of ω_{ij} and Ω is an important manifestation of the coherence transfer as discussed below. The decay rate of these oscillations at $\Omega=20$ cm^{-1}, which corresponds to the dephasing, was found to be $k_{ij,ji}+\gamma=1.0\pm0.1$ ps^{-1}. Similar decay rates were found for the oscillations of the coherence transfer components corresponding to the process matrix $\chi_{ji,ij}(T)$ and $\chi_{ij,ji}(T)$, as shown in Figures 3e,f. We, therefore, find from the definition of Ω that the pure dephasing rate is $\gamma\approx0.6$ ps^{-1} and the coherence transfer rate is $k_{ij,ji}\approx0.4$ ps^{-1}. The model in eq 9 predicts the amplitude of the coherence transfer oscillatory term of $k_{ij,ji}/\Omega\approx0.67$, which is fully consistent with the experimental results in Figures 3e,f, where the oscillation amplitude retrieved by QPT is 0.5 for the case of $\chi_{ji,ij}(T)$ and 0.75 for the case of $\chi_{ij,ji}(T)$ with the average value of $k_{ij,ji}/\Omega\approx0.63$.

In the interaction picture, the equation of motion 6 can be rewritten as

$$\dot{\rho}_{ij}^{I}(T)=\sum_{kl}R_{ij,kl}\rho_{kl}^{I}(T)\mathrm{e}^{-i(\omega_{ij}-\omega_{kl})T} \tag{11}$$

The population transfer elements $R_{ii,jj}$ of the relaxation matrix correspond to the secular terms of the equation, where $\omega_{ii}-\omega_{jj}=0$ always holds. For the coherence transfer, the secular approximation is valid if the inequality $R_{ji,ij}\ll|\omega_{ij}-\omega_{ji}|$ holds. In this case, upon the integration of eq 11, the contribution from the slow component corresponding to the coherence transfer rate is averaged out by fast oscillations at the frequency of $2\omega_{ij}$. The experimental rate constants obtained by QPT in the present study $k_{ij,ji}\approx0.4$ ps^{-1} and $2\omega_{ij}\approx0.7$ ps^{-1} clearly demonstrate the breakdown of the secular approximation because for the present case, the oscillations at the frequency of $2\omega_{ij}$ are not fast enough as compared to the rate of coherence transfer.[55]

QPT of Vibrational Exciton Dynamics: Simulation. In order to confirm that the QPT procedure applied to the vibrational exciton dynamics correctly retrieves the parameters of the population and coherence transfer during the waiting time, we tested the QPT performance by applying it to numerically simulated series of 2D-IR spectra, where we either included or omitted the contributions from the transfer processes. The simulations are based on the third-order response functions, which are schematically described by the double-sided diagrams shown in Figure 4. Because formal derivation of the response functions for the Liouville pathways involving the population and coherence transfer (see panels f,c) is not available, these pathways were included rather phenomenologically through the exponential prefactors derived in eqs 8 and 10 for the fully degenerate vibrational states. It is important to further stress here that although in the simulations we have used the parameters obtained from the experimental spectroscopic data of CHD, the response-function-simulated 2D-IR spectra do not rigorously represent dynamics driven by the master eq 7 because of the approximation involved in the transition between the eqs 9 and 10. Nevertheless, because the validation of our QPT implementation performance is highly important, we used these simulations as a test of the QPT protocol.

In the simulations we used $\omega_i=1710$ cm^{-1}, $\omega_j=1734$ cm^{-1}, $\mu_i^2/\mu_j^2=3$, and assumed frequency fluctuation correlation function $\xi_{ij}(t')=\langle\delta\omega_i(t')\delta\omega_j(0)\rangle$ ($\delta\omega_i$ is the frequency fluctuation of mode i) corresponding to Bloch dynamics $\xi_{ij}(t')=\Gamma\delta(t')+\sigma^2$, where Γ is the homogeneous and σ is the

dx.doi.org/10.1021/jp4075493 | J. Phys. Chem. B XXXX, XXX, XXX−XXX

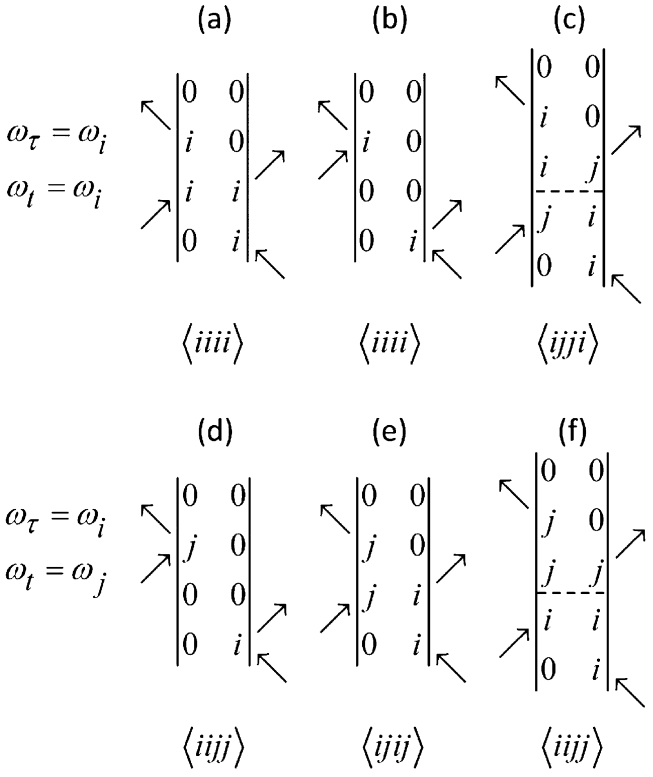

Figure 4. Double-sided diagrams illustrating Liouville pathways involved in the 2D-IR experiment that contribute to a photon-echo signal of two coupled oscillators at fundamental transitions. (a)−(c) Pathways contributing to the diagonal peaks $S_{ii}^{ABCD}(T)$. (d)−(f) Pathways contributing to the cross-peaks $S_{ij}^{ABCD}(T)$. The corresponding rotational factors are indicated below each pathway.

inhomogeneous broadening. The parameters of the autocorrelation function $\xi_{ii}(t') = \xi_{jj}(t')$ were chosen as $\Gamma = 0.5$ ps^{-1} and $\sigma = 0.5$ ps^{-1}. For the cross-correlation function, we used $\xi_{ij}(t') = 0.5\ \xi_{ii}(t')$. These simulation parameters were chosen to best reproduce the experimental 2D-IR spectra.

The reconstructed values of the process matrix elements $\chi_{ij,kl}(T)$ for the case where no transfer processes were included ($k_{ii,jj} = k_{ij,ji} = 0$) are shown in open dots in panels 1a−f of Figure 5, and red lines show the fits to the model described in eq 7. Here, the elements $\chi_{ii,ii}(T)$ and $\chi_{jj,jj}(T)$ corresponding to the populations are stationary and equal to unity during the waiting time evolution, and the elements $\chi_{jj,ii}(T)$ and $\chi_{ii,jj}(T)$ corresponding to the population transfer are zero. The elements $\chi_{ij,ij}(T)$ and $\chi_{ji,ji}(T)$ corresponding to the coherences show oscillatory behavior with exponential damping due to dephasing; the elements $\chi_{ji,ij}(T)$ and $\chi_{ij,ji}(T)$ corresponding to coherence transfer are zero. Results for the case where the transfer rates of $k_{ii,jj} = k_{ij,ji} = 0.5$ ps^{-1} were used are shown in panels 2a−f of Figure 5. In this case, fitting to the solution of eq 7 shows a very good agreement between the transfer rate constants used for the simulation and those retrieved by the QPT.

CONCLUSIONS

In conclusion, in the present study, we have applied QPT to experimentally quantify dynamics of the dissipative quantum states of the vibrational one-exciton manifold, which in addition to vibrational lifetime relaxation and rotational diffusion also involves dephasing and transfer of the vibrational excitation. QPT is a model-free approach that maps the density matrix elements before and after the free evolution one into another by means of linear transformation, providing an alternative to the modeling of system-bath interactions.

A vibrational exciton formed by the coupled carbonyl groups in CHD molecule undergoes dynamical processes induced by the interaction between the exciton and the fluctuating bath of the solvent. Excitation transfer phenomena are usually discussed within the framework of the Redfield theory and secular approximation, which significantly simplifies description of the complex system dynamics.[30,31,55] For example, secular approximation holds for the population transfer processes, whereas the process of the coherence transfer requires consideration of the nonsecular elements of the Redfield's relaxation operator.[31−33,42] Experimental quantification of the coherence transfer is highly challenging when approached by traditional ways of analyzing 2D spectra. Here, we find a good agreement between the results of the model-free QPT method

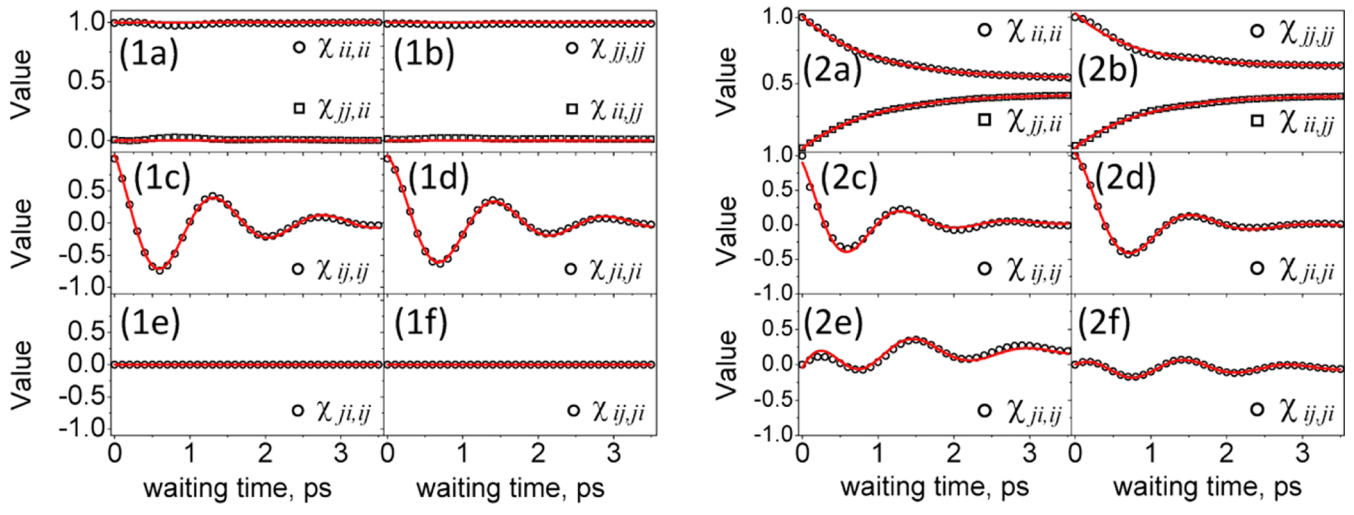

Figure 5. QPT of CHD: Simulation. Open dots are reconstructed elements of the process matrix $\chi_{ij,kl}(T)$. Red lines show fits of the results to the kinetic model on the basis of the Redfield's equation of motion. Panels 1a−f: no transfer process included ($k_{ii,jj} = k_{ij,ji} = 0$); panels 2a−f: population and coherence transfer included ($k_{ii,jj} = k_{ij,ji} = 0.5$ ps^{-1}). See text for details.

dx.doi.org/10.1021/jp4075493 | J. Phys. Chem. B XXXX, XXX, XXX−XXX

and solution of the Liouville−von Neumann equation of motion for an exciton coupled to Markovian bath. QPT, which is typically used in the field of quantum information, is experimentally demonstrated to be a powerful tool to separate and quantify individual contributions to the exciton dynamics, in particular to nonsecular process of the vibrational coherence transfer. The QPT conducted in the present work is partial in the sense that it does not include the processes of transfer between the populations and coherences and vice versa. Thus, in the corresponding nonsecular Redfield's theory description that we have used, the populations and coherences are not coupled and the density matrix equation of motion has an analytical solution where the population terms of the density matrix are always positive. For the experiments were the population-to-coherence transfer can be monitored, recently developed Lindblad equations method can be used.[59]

Along with the fundamental importance of our findings that reveal the solvation dynamics of the exciton in great detail, we expect that new kind of dynamical information made available by QPT will assist in solving many important questions by multidimensional spectroscopy where the relaxation phenomena in complex systems are extensively investigated. The fields of QPT applications may span from biomedical, focusing on drug−protein binding dynamics, to biophysical, focusing on the coherent energy transfer in light-harvesting antenna, to materials science. In this regard, studying the transfer phenomena associated with vibrational exciton dynamics in an aqueous environment is an important and challenging future direction.

■ ASSOCIATED CONTENT

Supporting Information

Parallel polarization absorptive spectrum and its projection. Measurements of vibrational lifetime and orientational diffusion of CHD in chloroform. This material is available free of charge via the Internet at http://pubs.acs.org.

■ AUTHOR INFORMATION

Corresponding Author

*L. Chuntonov. E-mail: chuntl@sas.upenn.edu. Phone: 215-898-8247. Fax: 215-898-0590.

Author Contributions

‡The authors contributed equally to the work.

Notes

The authors declare no competing financial interest.

■ ACKNOWLEDGMENTS

The authors acknowledge the idea of conducting QPT via 2D-IR to Professor Robin M. Hochstrasser, who led the Ultrafast Optical Processes Laboratory in the University of Pennsylvania until he passed away on February 27, 2013. Instrumentation used in this work was developed with a Research Resource grant from NIH (P41GM104605) to Robin M. Hochstrasser.

■ REFERENCES

(1) Fleming, G.; Huelga, S.; Plenio, M. Focus on Quantum Effects and Noise in Biomolecules. *New J. Phys.* **2011**, *13*, 115002.

(2) Hayes, D.; Griffin, G. B.; Engel, G. S. Engineering Coherence among Excited States in Synthetic Heterodimer Systems. *Science* **2013**, *340*, 1431−1434.

(3) Scholes, G. D. Quantum-Coherent Electronic Energy Transfer: Did Nature Think of It First? *J. Phys. Chem. Lett.* **2010**, *1*, 2−8.

(4) Collini, E.; Scholes, G. D. Coherent Intrachain Energy Migration in a Conjugated Polymer at Room Temperature. *Science* **2009**, *323*, 369−373.

(5) Fidler, A. F.; Caram, J. R.; Hayes, D.; Engel, G. S. Towards a Coherent Picture of Excitonic Coherence in the Fenna−Matthews−Olson Complex. *J. Phys. B* **2012**, *45*, 154013.

(6) Hildner, R.; Brinks, D.; Nieder, J. B.; Cogdell, R. J.; van Hulst, N. F. Quantum Coherent Energy Transfer over Varying Pathways in Single Light-Harvesting Complexes. *Science* **2013**, *340*, 1448−1451.

(7) Shapiro, M.; Brumer, P. *Principles of the Quantum Control of Molecular Processes*; Wiley-VCH: Weinheim, Germany, 2003.

(8) Mukamel, S. *Principles of Nonlinear Optical Spectroscopy*; Oxford University Press: New York, 1999.

(9) Cho, M. *Two-Dimensional Optical Spectroscopy*; Taylor & Francis: Boca Raton, FL, 2010.

(10) Hamm, P.; Zanni, M. T. *Concepts and Methods of 2d Infrared Spectroscopy*; Cambridge University Press: Cambridge, U. K., 2011.

(11) Mukamel, S. Multidimensional Femtosecond Correlation Spectroscopies of Electronic and Vibrational Excitations. *Annu. Rev. Phys. Chem.* **2000**, *51*, 691−729.

(12) de Boeij, W. P.; Pshenichnikov, M. S.; Wiersma, D. A. Ultrafast Solvation Dynamics Explored by Femtosecond Photon Echo Spectroscopies. *Annu. Rev. Phys. Chem.* **1998**, *49*, 99−123.

(13) Cho, M.; Yu, J.-Y.; Joo, T.; Nagasawa, Y.; Passino, S. A.; Fleming, G. R. The Integrated Photon Echo and Solvation Dynamics. *J. Phys. Chem.* **1996**, *100*, 11944−11953.

(14) Khalil, M.; Demirdöven, N.; Tokmakoff, A. Coherent 2d Ir Spectroscopy: Molecular Structure and Dynamics in Solution. *J. Phys. Chem. A* **2003**, *107*, 5258−5279.

(15) Kuroda, D. G.; Bauman, J. D.; Challa, J. R.; Patel, D.; Troxler, T.; Das, K.; Arnold, E.; Hochstrasser, R. M. Snapshot of the Equilibrium Dynamics of a Drug Bound to Hiv-1 Reverse Transcriptase. *Nature Chem.* **2013**, *5*, 1755−4330.

(16) Kim, Y. S.; Liu, L.; Axelsen, P. H.; Hochstrasser, R. M. 2d Ir Provides Evidence for Mobile Water Molecules in B−Amyloid Fibrils. *Proc. Nat. Acad. Sci. U. S. A.* **2009**, *106*, 17751−17756.

(17) Ghosh, A.; Qiu, J.; DeGrado, W. F.; Hochstrasser, R. M. Tidal Surge in the M2 Proton Channel, Sensed by 2d Ir Spectroscopy. *Proc. Nat. Acad. Sci. U. S. A.* **2011**, *108*, 6115−6120.

(18) Kim, Y. S.; Hochstrasser, R. M. Chemical Exchange 2d Ir of Hydrogen-Bond Making and Breaking. *Proc. Nat. Acad. Sci. U. S. A.* **2005**, *102*, 11185−11190.

(19) Ishikawa, H.; Kwak, K.; Chung, J. K.; Kim, S.; Fayer, M. D. Direct Observation of Fast Protein Conformational Switching. *Proc. Nat. Acad. Sci. U. S. A.* **2008**, *105*, 8619−8624.

(20) Maekawa, H.; Ge, N.-H. Picosecond Rotational Interconversion Adjacent to a C═O Bond Studied by Two-Dimensional Infrared Spectroscopy. *J. Phys. Chem. B* **2012**, *116*, 11292−11301.

(21) Kim, Y. S.; Hochstrasser, R. M. Applications of 2d Ir Spectroscopy to Peptides, Proteins, and Hydrogen-Bond Dynamics. *J. Phys. Chem. B* **2009**, *113*, 8231−8251.

(22) Thielges, M. C.; Fayer, M. D. Protein Dynamics Studied with Ultrafast Two-Dimensional Infrared Vibrational Echo Spectroscopy. *Acc. Chem. Res.* **2012**, *45*, 1866−1874.

(23) Wong, D. B.; Giammanco, C. H.; Fenn, E. E.; Fayer, M. D. The Dynamics of Isolated Water Molecules in a Sea of Ions in a Room Temperature Ionic Liquid. *J. Phys. Chem. B* **2012**, *117*, 623−635.

(24) Xiong, W.; Laaser, J. E.; Mehlenbacher, R. D.; Zanni, M. T. Adding a Dimension to the Infrared Spectra of Interfaces Using Heterodyne Detected 2d Sum-Frequency Generation (Hd 2d Sfg) Spectroscopy. *Proc. Nat. Acad. Sci. U. S. A.* **2011**, *108*, 20902−20907.

(25) Chuntonov, L.; Kuroda, D. G.; Ghosh, A.; Ma, J.; Hochstrasser, R. M. Quantum Beats and Coherence Decay in Degenerate States Split by Solvation. *J. Phys. Chem. Lett.* **2013**, *4*, 1866−1871.

(26) Hochstrasser, R. M. Electronic Spectra of Organic Molecules. *Annu. Rev. Phys. Chem.* **1966**, *17*, 457−480.

(27) Robinson, G. W. Electronic and Vibrational Excitons in Molecular Crystals. *Annu. Rev. Phys. Chem.* **1970**, *21*, 429−474.

(28) Skinner, J. L.; Andersen, H. C.; Fayer, M. Theory of Photon Echoes from a Pair of Coupled Two Level Systems: Impurity Dimers and Energy Transfer in Molecular Crystals. *J. Chem. Phys.* **1981**, *75*, 3195.
(29) Wertheimer, R.; Silbey, R. On Excitation Transfer and Relaxation Models in Low-Temperature Systems. *Chem. Phys. Lett.* **1980**, *75*, 243−248.
(30) Redfield, A. G. On the Theory of Relaxation Processes. *IBM J. Res. Dev.* **1957**, *1*, 19−31.
(31) Nitzan, A. *Chemical Dynamics in Condensed Phases: Relaxation, Transfer and Reactions in Condensed Molecular Systems*; OUP: Oxford, U. K., 2006.
(32) Khalil, M.; Demirdoven, N.; Tokmakoff, A. Vibrational Coherence Transfer Characterized with Fourier-Transform 2d Ir Spectroscopy. *J. Chem. Phys.* **2004**, *121*, 362−373.
(33) Nee, M. J.; Baiz, C. R.; Anna, J. M.; McCanne, R.; Kubarych, K. J. Multilevel Vibrational Coherence Transfer and Wavepacket Dynamics Probed with Multidimensional Ir Spectroscopy. *J. Chem. Phys.* **2008**, *129*, 084503−084511.
(34) Pakoulev, A. V.; Rickard, M. A.; Kornau, K. M.; Mathew, N. A.; Yurs, L. A.; Block, S. B.; Wright, J. C. Mixed Frequency-/Time-Domain Coherent Multidimensional Spectroscopy: Research Tool or Potential Analytical Method? *Acc. Chem. Res.* **2009**, *42*, 1310−1321.
(35) Wright, J. C. Multiresonant Coherent Multidimensional Spectroscopy. *Annu. Rev. Phys. Chem.* **2011**, *62*, 209−230.
(36) Baiz, C. R.; Kubarych, K. J.; Geva, E. Molecular Theory and Simulation of Coherence Transfer in Metal Carbonyls and Its Signature on Multidimensional Infrared Spectra. *J. Phys. Chem. B* **2011**, *115*, 5322−5339.
(37) Ghosh, A.; Tucker, M. J.; Hochstrasser, R. M. Identification of Arginine Residues in Peptides by 2d-Ir Echo Spectroscopy. *J. Phys. Chem. A* **2011**, *115*, 9731−9738.
(38) Park, S.; Ji, M. Ultrafast Vibrational Population Transfer Dynamics in 2−Acetylcyclopentanone Studied by 2d Ir Spectroscopy. *ChemPhysChem* **2011**, *12*, 799−805.
(39) Son, H.; Park, K.-H.; Kwak, K.-W.; Park, S.; Cho, M. Ultrafast Intermolecular Vibrational Excitation Transfer from Solute to Solvent: Observation of Intermediate States. *Chem. Phys.* **2013**, *422*, 37−46.
(40) Vorobyev, D. Y.; Kuo, C.-H.; Chen, J.-X.; Kuroda, D. G.; Scott, J. N.; Vanderkooi, J. M.; Hochstrasser, R. M. Ultrafast Vibrational Spectroscopy of a Degenerate Mode of Guanidinium Chloride. *J. Phys. Chem. B* **2009**, *113*, 15382−15391.
(41) Vorobyev, D. Y.; Kuo, C.-H.; Kuroda, D. G.; Scott, J. N.; Vanderkooi, J. M.; Hochstrasser, R. M. Water-Induced Relaxation of a Degenerate Vibration of Guanidinium Using 2d Ir Echo Spectroscopy. *J. Phys. Chem. B* **2010**, *114*, 2944−2953.
(42) Pakoulev, A. V.; Rickard, M. A.; Mathew, N. A.; Kornau, K. M.; Wright, J. C. Frequency-Domain Time-Resolved Four Wave Mixing Spectroscopy of Vibrational Coherence Transfer with Single-Color Excitation. *J. Phys. Chem. A* **2008**, *112*, 6320−6329.
(43) King, J. T.; Anna, J. M.; Kubarych, K. J. Solvent-Hindered Intramolecular Vibrational Redistribution. *Phys. Chem. Chem. Phys.* **2011**, *13*, 5579−5583.
(44) Kuroda, D. G.; Singh, P. K.; Hochstrasser, R. M. Differential Hydration of Tricyanomethanide Observed by Time Resolved Vibrational Spectroscopy. *J. Phys. Chem. B* **2012**, *117*, 4354−4364.
(45) Rubtsov, I. V. Relaxation-Assisted Two-Dimensional Infrared (Ra 2dir) Method: Accessing Distances over 10 Å and Measuring Bond Connectivity Patterns. *Acc. Chem. Res.* **2009**, *42*, 1385−1394.
(46) Falvo, C.; Sanda, F.; Mukamel, S. Quasi-Particle Approach to 2d Ir Spectra of Vibrational Excitons in Biomolecules. In *Ultrafast Infrared Vibrational Spectroscopy*; Fayer, M. D., Ed.; CRC Press: Boca Raton, FL, 2013; pp 405.
(47) Ge, N.-H.; Zanni, M. T.; Hochstrasser, R. M. Effects of Vibrational Frequency Correlations on Two-Dimensional Infrared Spectra. *J. Phys. Chem. A* **2001**, *106*, 962−972.
(48) Sanda, F.; Mukamel, S. Stochastic Liouville Equations for Coherent Multidimensional Spectroscopy of Excitons. *J. Phys. Chem. B* **2008**, *112*, 14212−14220.
(49) Yuen-Zhou, J.; Aspuru-Guzik, A. Quantum Process Tomography of Excitonic Dimers from Two-Dimensional Electronic Spectroscopy. I. General Theory and Application to Homodimers. *J. Chem. Phys.* **2011**, *134*, 134505.
(50) Yuen-Zhou, J.; Krich, J. J.; Mohseni, M.; Aspuru-Guzik, A. Quantum State and Process Tomography of Energy Transfer Systems Via Ultrafast Spectroscopy. *Proc. Nat. Acad. Sci. U. S. A.* **2011**, *108*, 17615−17620.
(51) Yuen-Zhou, J.; Arias, D. H.; Eisele, D. M.; Steiner, C. P.; Krich, J. J.; Bawendi, M.; Nelson, K. A.; Aspuru-Guzik, A. Coherent Exciton Dynamics in Supramolecular Light-Harvesting Nanotubes Revealed by Ultrafast Quantum Process Tomography. *Cornell University Library* **2013**, No. arXiv:1308.4566.
(52) Chuang, I. L.; Nielsen, M. Prescription for Experimental Determination of the Dynamics of a Quantum Black Box. *J. Mod. Opt.* **1997**, *44*, 2455−2467.
(53) Nielsen, M. A.; Chuang, I. L. *Quantum Computation and Quantum Information*; Cambridge University Press: Cambridge, U. K., 2010.
(54) Ma, X.-S.; Herbst, T.; Scheidl, T.; Wang, D.; Kropatschek, S.; Naylor, W.; Wittmann, B.; Mech, A.; Kofler, J.; Anisimova, E. Quantum Teleportation over 143 Kilometres Using Active Feed-Forward. *Nature* **2012**, *489*, 269−273.
(55) Ishizaki, A.; Fleming, G. R. On the Adequacy of the Redfield Equation and Related Approaches to the Study of Quantum Dynamics in Electronic Energy Transfer. *J. Chem. Phys.* **2009**, *130*, 234110.
(56) Zanni, M. T.; Ge, N.-H.; Kim, Y. S.; Hochstrasser, R. M. Two-Dimensional Ir Spectroscopy Can Be Designed to Eliminate the Diagonal Peaks and Expose Only the Crosspeaks Needed for Structure Determination. *Proc. Nat. Acad. Sci. U. S. A.* **2001**, *98*, 11265−11270.
(57) Hochstrasser, R. M. Two-Dimensional Ir-Spectroscopy: Polarization Anisotropy Effects. *Chem. Phys.* **2001**, *266*, 273−284.
(58) Fang, C.; Wang, J.; Kim, Y. S.; Charnley, A. K.; Barber-Armstrong, W.; Smith, A. B.; Decatur, S. M.; Hochstrasser, R. M. Two-Dimensional Infrared Spectroscopy of Isotopomers of an Alanine Rich Alpha-Helix. *J. Phys. Chem. B* **2004**, *108*, 10415−10427.
(59) Palmieri, B.; Abramavicius, D.; Mukamel, S. Lindblad Equations for Strongly Coupled Populations and Coherences in Photosynthetic Complexes. *J. Chem. Phys.* **2009**, *130*, 204512.